Journal of Environmental Chemical Engineering 10 (2022) 107435

Contents lists available at ScienceDirect

Journal of Environmental Chemical Engineering

journal homepage: www.elsevier.com/locate/jece

Insights into the performance, mechanism, and ecotoxicity of levofloxacin degradation in $CoFe_2O_4$ catalytic peroxymonosulfate process

Lili Liu [a], Rui Zhan [a], Meng Zhang [a,b,*], Jianan Li [a], Zhiping Wang [c,**], Haosheng Mi [a], Yunxiao Zhang [a]

[a] State Environmental Protection Key Laboratory of Environmental Risk Assessment and Control on Chemical Process, School of Resource and Environmental Engineering, East China University of Science and Technology, Shanghai 200237, PR China
[b] State Key Laboratory of Environmental Geochemistry, Institute of Geochemistry, Chinese Academy of Sciences, Guiyang 550081, PR China
[c] School of Environment Science and Technology, Shanghai Jiao Tong University, Shanghai 200240, PR China

ARTICLE INFO

Editor: Dong-Yeun Koh

Keywords:
Levofloxacin
$CoFe_2O_4$
Peroxymonosulfate
Reaction mechanisms
Ecotoxicity assessment

ABSTRACT

The catalysis effectiveness and influence factors of $CoFe_2O_4$ nanoparticles were investigated with peroxymonosulfate (PMS) as oxidant. Meanwhile, the degradation mechanism of levofloxacin (LVF) and the toxicity of its degradation products were analyzed. Efficient LVF degradation (95.4%) could be achieved within 30 min in $CoFe_2O_4$/PMS system with the optimum reaction conditions. The removal efficiency of LVF was decreased from 94.66% to 27.38% as the concentration of HCO_3^- increased from 0 to 20 mM, while increased to nearly 100% with 5 mM $H_2PO_4^-$ addition. The inhibition effect of Cl^- on LVF removal decreased as the concentration of Cl^- increased, and the addition of humic acid did not affect the final removal efficiency of LVF significantly. According to the results of degradation experiments and XPS analysis, both ═Co(II)/═Co(III) and ═Fe(II)/═Fe(III) redox pairs were involved in PMS catalysis, and ═Co(II)/═Co(III) played a dominant role. $SO_4^{\bullet-}$ was the dominant free radical in $CoFe_2O_4$/PMS system for LVF degradation, and five possible degradation pathways were proposed based on the eleven degradation products. Compared with LVF, more toxic degradation products were generated in degradation pathways of decarboxylation and conversion of quinolone moieties, due to the coexisting of $SO_4^{\bullet-}$ and HO•. Meanwhile, the luminescence inhibition ratio of the reaction solution (23.5%) was still higher than the original LVF solution (21.4%) by the end of the experiment. Therefore, the degradation pathways that generate toxic products should be avoided or detoxification by the complete mineralization of LVF, which needs further research via the targeted optimization of $CoFe_2O_4$/PMS system.

1. Introduction

Fluoroquinolones (FQs) are widely used antibiotics for the treatment of bacterial infections in humans and livestock [1]. The accumulation of FQs in environmental media have received considerable critical attention [2], in consideration of the induce generation of antibiotic resistance genes [3]. As one of the currently FDA-approved FQs for the treatment of nosocomial pneumonia [4], Levofloxacin (LVF) has been widely detected in pharmaceutical effluents. The average concentration of LVF in the waste-water of Pakistan is in the range of 36.7–48.9 μg/L, and much higher (91.0～164.0 μg/kg) in the sludge [5]. The released LVF eventually discharges into water bodies, which may result in water pollution and pose hazards to aquatic organisms and human. According to the previous studies for FQs in aquatic environments in China, the median concentration of LVF is 23.40 ng/L [6]. In view of the low degradation rate of FQs by conventional sewage treatment process and natural microbial degradation, the development of efficient degradation method is urgent [7].

Advanced oxidation processes (AOPs) that base on the production of reactive radicals can degrade antibiotics effectively [8–11]. Meanwhile, sulfate radical ($SO_4^{\bullet-}$) characterized by high redox potential, long half-life period, wider applicable pH range, and high selectivity has gained wide attention and application [12–15]. Although the cobalt ions (Co^{2+}) are more effective at decomposing PMS into $SO_4^{\bullet-}$ for the removal of refractory organic pollutants compared with other transition metal ions, the direct release of Co^{2+} into water has a considerable

* Correspondence to: 130 Meilong Road, Shanghai, PR China.
** Corresponding author.
E-mail addresses: zhangmeng@ecust.edu.cn (M. Zhang), wangzply@sjtu.edu.cn (Z. Wang).

https://doi.org/10.1016/j.jece.2022.107435
Received 14 December 2021; Received in revised form 5 February 2022; Accepted 16 February 2022
Available online 18 February 2022

impact on aquatic ecosystem and humans. As a result, researches about the stable cobalt-based solid catalysts have gained a lot of attention [16]. The cobalt ferrite ($CoFe_2O_4$) nanoparticles (NPs) have been successfully used for PMS activization to degrade antibiotics, including sulfamethoxazole [17], ciprofloxacin [18], moxifloxacin [19], and norfloxacin [20], et al. Meanwhile, studies have confirmed that the surface metal redox couples are the main reasons for the high catalytic activity of $CoFe_2O_4$ [21,22], and the Co leaching can be markedly suppressed due to Fe–Co interactions [23]. However, the completely mineralize of micro-organic pollutants by $CoFe_2O_4$/PMS system is difficult, thus the toxicity assessment of the degradation products is very important [24].

The catalytic oxidation of LVF based on microwave–3D $ZnCo_2O_4$ and electrocatalyst (CQDs@FeOOH nanoneedles) have been investigated, and the acute toxicities of degradation intermediates are verified base on the luminous bacteria tests [25,26]. The algae (*Chlorella vulgaris*) growth inhibition toxicity increased with the reaction (MnOx/SBA-15/O_3) time, indicating the formation of high-toxic degrade intermediates [27]. In addition, besides the above-mentioned biological toxicity test methods, Ecological Structure−Activity Relationship Model (ECOSAR) program that based on the definite chemical structures of target pollutants, can also be used for the toxicity assessment of oxidative degradation products of antibiotics [24,28]. However, limited studies have been conducted to assess the toxicity of reaction solutions of FQs after $SO_4^{\bullet-}$-based treatment processes [29]. It has been reported that the oxo-quinolinecarboxylic acid structure will be retained in most of the degrade intermediates of FQs after metal-mediated $SO_4^{\bullet-}$-based treatment, which raised concerns about the residual antimicrobial activity [30].

In such circumstances, $CoFe_2O_4$ nanoparticles (NPs) was synthesized by citric acid-assisted sol-gel method, and used for the PMS activation to degrade LVF. In order to verify the catalyst effectiveness of the $CoFe_2O_4$ NPs, the degradation experiments were performed with the optimal PMS dosage. Meanwhile, the impact of inorganic anions (Cl^-, HCO_3^-, $H_2PO_4^-$) and humic acids on catalytic oxidation reaction have been also investigated. The main radical species that involved in LVF degradation, the degradation products and their corresponding toxicity were analyzed. The research conclusion can provide a new perspective for specific heterogeneous catalytic oxidation to effectively reduce toxic degradation product.

2. Material and methods

2.1. Chemicals

Levofloxacin (LVF, 98%), ethanol (EtOH, 99.8%) and tert-butanol (TBA, 99.5%) were obtained from Shanghai Macklin Biochemical Co., Ltd, Shanghai, China. PMS, known as Oxone ($KHSO_5{\cdot}KHSO_4{\cdot}K_2SO_4$, ≥47% $KHSO_5$ basis), $Fe(NO_3)_3{\cdot}9H_2O$ (97%), and $Co(NO_3)_3{\cdot}6H_2O$ (99%) were obtained from Shanghai Aladdin Biochemical Co., Ltd, Shanghai, China. NaCl (99.5%), NaH_2PO_4(99%), $NaHCO_3$ (99.8%), and Humic acid (HA) were purchased from Lingfeng Chemical Reagent Co., Ltd, Shanghai, China. All chemical reagents used in the experiments were analytical grade and all solutions were prepared using ultrapure water.

2.2. Preparation and characterization of $CoFe_2O_4$ NPs

The $CoFe_2O_4$ NPs was synthesized by citric acid-assisted sol-gel method [31]. In detail, $Co(NO_3)_2{\cdot}6H_2O$ and $Fe(NO_3)_3{\cdot}9H_2O$ were dissolved in ultrapure water in a molar ratio of 1:2, and stirred in a water bath at a constant temperature of 60 °C for two hours, then citric acid with a molar concentration equal to the sum of the molar concentrations of the metal ions was added as a complexing agent. The mixture was then stirring and heated in an oil bath at 120 °C, and a honeycomb dry gel was obtained after five hours. The obtained catalyst was grinding into powder and calcining in a muffle furnace at 400 °C for 2 h.

Characterization of the external surface microstructure and crystal structure of the $CoFe_2O_4$ NPs were performed using field emission scanning electron microscopy (GeminiSEM 500, Carl Zeiss AG, Germany) and rotating anode X-ray powder diffractometer (XRD, 18KW/D/max2550VB/PC, Rigaku Corporation, Japan), respectively. Brunauer-Emmett-Teller (BET) surface area was examined by using a TriStar II 3020 (Micromeritics, USA) instrument (N_2 adsorption, 77 K). Chemical states of Co, Fe and O were studied by X-ray photoelectron spectroscopy (ESCALAB 250Xi, Thermo Fisher Scientific, USA).

2.3. Degradation experiment

The LVF degradation experiments were carried out in 250 mL glass Erlenmeyer flasks (pH=7.0 ± 0.1) at room temperature (25 °C) with continuous stirring at 170 rpm. All tests are performed in triplicate, and the results are averaged values of the three samples.

The reaction is initiated by adding a certain volume of PMS stock solution and a certain mass of $CoFe_2O_4$ NPs to the LVF solution. 1 mL of the reaction mixture was accurately collected at predetermined time intervals and filtered by a 0.22 μm PES membrane, then 0.2 mL NaS_2O_3 solution (0.1 M) was immediately added to quench the oxidation reactions. The quenching experiments were carried out to determine the involved free radicals, with the initial excess addition of TBA and EtOH to the reaction system. The specified concentrations of inorganic anions (Cl^-, HCO_3^-, $H_2PO_4^-$) and HA were added into the reaction system to determine their influence. The catalyst was magnetically separated and subsequently washed several times with distilled water and then dried at 60 °C.

2.4. Analytical methods

A Shimadzu LC-20AT high performance liquid chromatographic system equipped with a C18 reversed-phase column and a variable wavelength UV detector (detection wavelength: 293 nm) was used for the quantitative analysis of residual LVF in solution. The mobile phase was phosphoric acid and methanol mixed in the ratio of 40:60 (V/V) at a flow rate of 1 mL/min. The concentration of leached metal ions was measured by a laboratory spectrophotometer (DR3900, HACH, USA). LVF degradation products was identified by ultra performance liquid chromatography (ultimate 3000) -mass spectrometry (Q-Exactive™ plus). OriginPro 2019 (Origin Lab, USA) was used for experimental data plotting.

2.5. Ecotoxicity assessment

The acute and chronic toxicity of LVF and its degradation products were predicted by the ECOSAR program, which has been ranked as one of the most effective predictive programs for organics toxicity [32]. The molecular weight of LVF is within the applicable range of ECOSAR (Mw<1000). For acute toxicity, 96-h Half Lethal Concentration (LC_{50}, mg/L) for fish, 48-h Half Lethal Concentration for Daphnia, and 96-h Half Effective Concentration (EC_{50}, mg/L) for green algae were estimated, respectively. Moreover, the chronic toxicity of LVF and its degradation products were assessed in terms of ChV values (mg/L) to fish, daphnia, and green algae, severally.

3. Results and discussion

3.1. Characterizations of $CoFe_2O_4$ NPs

FESEM image indicated uniform three-dimensional nanoparticles (NPs) of the synthesized $CoFe_2O_4$ (Fig. 1a), and the homogeneous distribution of the NPs with mean size of 14.8 ± 2.9 nm (Fig. 1b, inset) could also be observed in TEM image (Fig. 1b). The XRD pattern of the $CoFe_2O_4$ NPs is shown in Fig. 1c, eight characteristic peaks at 18.3°, 30.1°, 35.4°, 43.1°, 53.4°, 57.0°, 62.6°, 74.0° that in good agreement

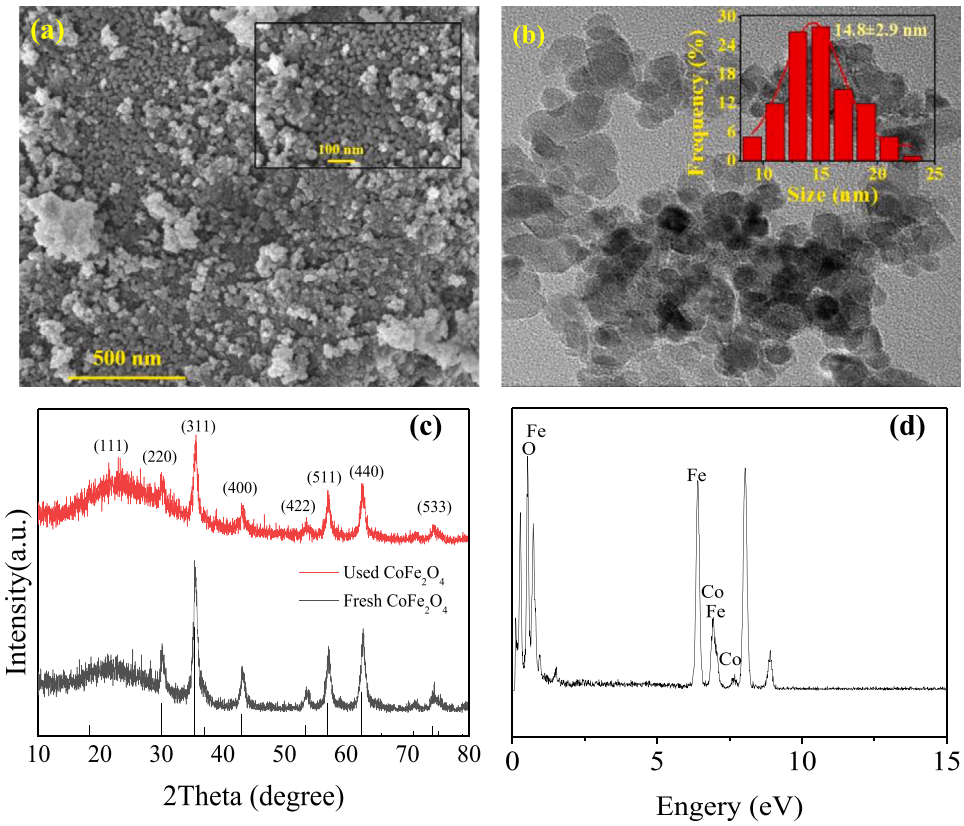

Fig. 1. FE-SEM images (a), TEM images (b), XRD pattern (c), EDS pattern (d) of the synthesized $CoFe_2O_4$ NPs.

with the crystal planes (1 1 1), (2 2 0), (3 1 1), (4 0 0), (4 2 2), (5 1 1), (4 4 0) and (5 3 3) were observed, which is in accordance with the spinel $CoFe_2O_4$ (JCPDS: 22–1086) [33,34]. Moreover, no impurity peaks were observed implies the superior purity of $CoFe_2O_4$ NPs [33,35]. Meanwhile, the XRD patterns of $CoFe_2O_4$ NPs were essentially unchanged before and after the reaction, indicating its structural stability. According to the EDS analysis results (Fig. 1d), the molar ratio of Co to Fe in $CoFe_2O_4$ NPs is 9.67%: 22.59%, which is close to 1:2. The nitrogen adsorption-desorption isotherm (Fig. S1) was standard IV-type, and the BET surface area of the synthesized $CoFe_2O_4$ NPs was 53.3 m^2/g.

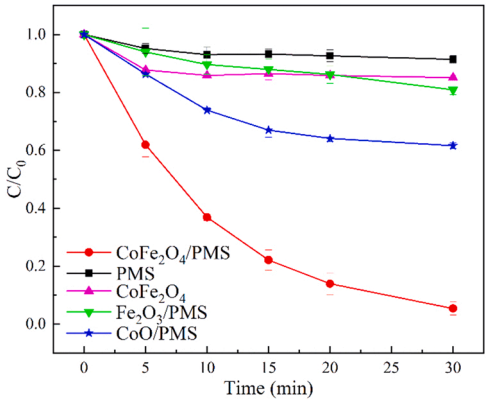

Fig. 2. Degradation of LVF in different experiments (reaction conditions: [$CoFe_2O_4$] / [Fe_2O_3] / [CoO] =100 mg/L, [PMS]=0.25 mM, [LVF]=5 mg/L, pH_0 =7, T = 25 °C).

3.2. LVF removal in $CoFe_2O_4$/PMS heterogeneous catalytic system

3.2.1. Degradation of LVF in different experiments

The removal efficiencies of LVF in different experiment were shown in Fig. 2. The removal efficiency of LVF in PMS alone and $CoFe_2O_4$ NPs alone experiment was 8.57% and 14.90%, respectively, indicating the weak oxidation capacity of PMS without activization and the adsorption capacity of $CoFe_2O_4$ NPs. The removal efficiency of LVF in Fe_2O_3/PMS, CoO/PMS, and $CoFe_2O_4$/PMS experiment was 19.15%, 38.42%, 94.63%, respectively, and the corresponding apparent rate constants (k_{obs}, fitted by the pseudo first-order model) was 0.0066 min^{-1}, 0.0163 min^{-1}, 0.0997 min^{-1} (Fig. S2). Similar results are obtained in heterogeneous Fenton reaction system, the removal efficiency of doxycycline follow the order of $CoFe_2O_4/H_2O_2$ > CoO + Fe_2O_3/H_2O_2 > CoO/H_2O_2 > Fe_2O_3/H_2O_2 > H_2O_2 [36]. The removal efficiency of LVF still can achieve 58.11% after five cycles of the $CoFe_2O_4$ NPs, and the cumulative dissolving quantity of Co and Fe was 0.66 mg/L and 0.16 mg/L, respectively (Fig. S3), indicating the good reusability and stability. The surface ≡Co(II)/≡Co(III) and ≡Fe(II)/≡Fe(III) redox pairs are the main reasons for efficient catalytic decomposition of PMS [16,37,38]. Meanwhile, the interaction between ≡Co and ≡Fe may be responsible for the high catalytic property of the $CoFe_2O_4$ NPs.

3.2.2. Factors that affect LVF removal in $CoFe_2O_4$/PMS system

3.2.2.1. The initial solution pH, catalyst and PMS dosage. The initial solution pH (pH_0) can significantly affect the speciation of organic compounds, the generation of free radicals, and the surface charges of catalysts [2,39,40], which will further influence the catalytic oxidation efficiency of organic contaminants. The effect of pH_0 (3, 5, 7, 9, 11) on the removal efficiency of LVF in $CoFe_2O_4$/PMS system is shown in Fig. 3a. There was no significant difference in the ultimate degradation rate of LVF (≈95%) when pH_0 increased from 5 to 9, while the

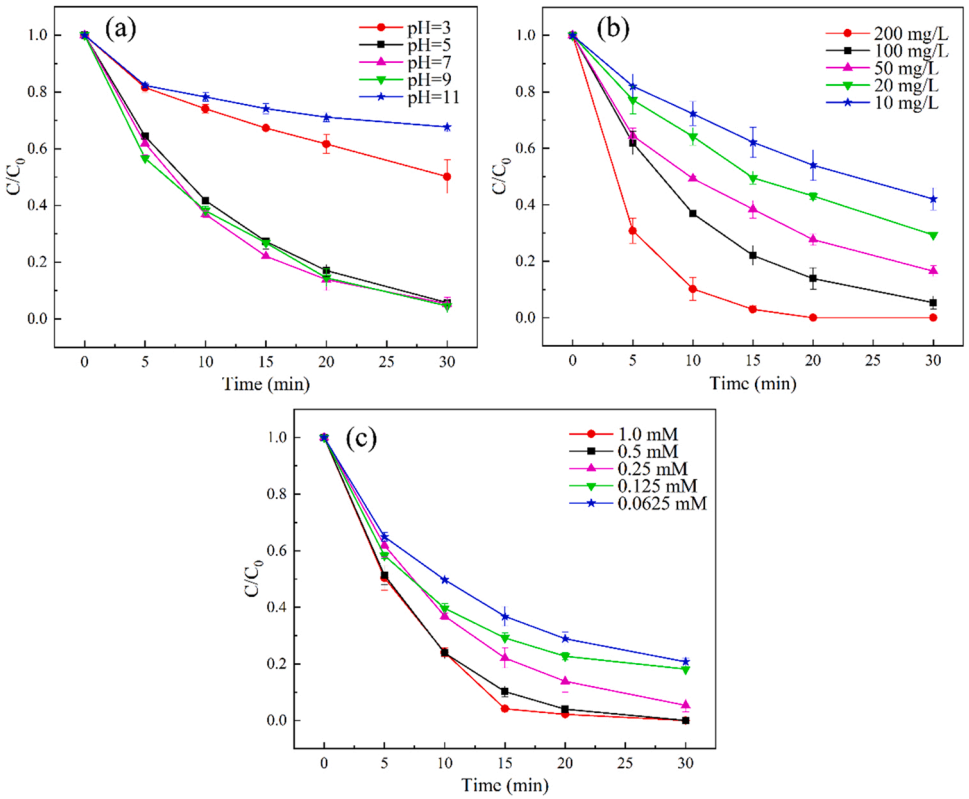

Fig. 3. Effect of pH (a), catalyst dosage (b), and PMS concentration (c) on the removal of LVF (reaction conditions of Fig. a and Fig. c: [$CoFe_2O_4$] =100 mg/L, [PMS]=0.25 mM, [LVF]=5 mg/L, pH_0 =7, T = 25 °C).

corresponding k_{obs} value gradually increased from 0.0881 to 0.1023 min^{-1} (Fig. S4). However, the degradation of LVF was significantly inhibited in the condition of pH_0 = 3 (49.85%) and pH_0 = 11 (32.30%), respectively, and corresponding k_{obs} value was just 0.0224 and 0.0117 min^{-1}.

The reported pKa1 value of PMS is less than 0 and the pKa2 value is about 9.4 [41]. Therefore, H_2SO_5 is the available specie form under extreme acidic conditions (pH=3), thus affecting the generation of sulfate radicals [31]. Meanwhile, the generation of ≡Co(II)-OH^+ will be severely inhibited at pH= 3 (Eq. (1)), thus result in the low activation efficiency of PMS [42]. In addition, according to Eqs. (2) and (3), the HO• and $SO_4^{\bullet-}$ radical species can also be trapped by hydrogen ions at low pH levels and participate in non-radical or less-powerful radical generating processes [43]. In addition, when the systematic pH increases above 11, $SO_4^{\bullet-}$ will be scavenged by OH^- and HO• become the dominant free radical (Eqs. (4) and (5)), cause the LVF removal efficiency decrease [44]. Simultaneously, large amount of cobalt hydroxide complexes will be generated at higher pH and adhered to the catalyst surface, resulting in the decrease of catalyst activity of $CoFe_2O_4$ NPs [22, 45,46]. Moreover, the surface charge of $CoFe_2O_4$ NPs is negative or positive when the pH is above or below its pH_{pzc} (5.96) [47,48]. When the system pH= 3, the positively charged catalyst surface has a strong electrostatic repulsion to the dissociated LVF (pKa1 =5.33, pKa2 =8.07). Therefore, little amount of LVF can be absorbed and degraded on the $CoFe_2O_4$ NPs surface, and the same applies at pH= 11 [30,49]. Furthermore, in the condition of high pH levels, PMS may decompose into H_2O and SO_4^{2-} via Eq. (6) [50,51].

$$\equiv \mathrm{II}) + H_2O \rightarrow \equiv \mathrm{II})\text{-}OH^+ + H^+ \quad (1)$$

$$HO\bullet + H^+ + e^- \rightarrow H_2O \quad (2)$$

$$SO4\bullet^- + H^+ + e^- \rightarrow HSO4\bullet^- \quad (3)$$

$$SO4\bullet^- + OH^- \rightarrow HO\bullet + SO_4^{2-} \quad k = (6.5 \pm 1.0) \times 10^7 M^{-1}s^{-1} \quad (4)$$

$$SO_4^{\bullet-} + H_2O \rightarrow HO\bullet + SO_4^{2-} + H^+ \quad k[H_2O] < 3.0 \times 10^3 M^{-1}s^{-1} \quad (5)$$

$$HSO_5^- + SO_5^{2-} + OH^- \rightarrow 2SO_4^{2-} + O_2 + H_2O \quad (6)$$

Meanwhile, the variation of solution pH has been monitored in $CoFe_2O_4$/PMS system with the optimum reaction conditions (Fig. S5). The solution pH decreased to approximately 4.4 during the first 5 min, and then leveled off. The H^+ will be released into the reaction solution through Eqs. (7) and (8), when the desired PMS dose is added [52]. Similar result is obtained in the degradation of atrazine through $CoFe_2O_4$ (400 mg/L) activated PMS (0.8 mM) process (pH_0 =6.3), the solution pH sharply decreased to almost 3.0 and level off during the 30 min treatment [53].

$$HSO_5^- \rightarrow H^+ + SO_5^{2-} \quad (7)$$

$$HSO_5^- + H_2O \rightarrow H_2O_2 + HSO_4^- \quad (8)$$

The effect of catalyst dosage on LVF removal is shown in Fig. 3b. As the catalyst dosage increased from 10 mg/L to 200 mg/L, the degradation efficiency of LVF increased from 57.98% to nearly 100%, and the k_{obs} value increased from 0.0291 min^{-1} to 0.2367 min^{-1} (Fig. S4). As the source of reactive species such as $SO_4^{\bullet-}$ and HO•, PMS plays a crucial role in the degradation of LVF. It was observed that the higher the PMS concentration, the better the degradation of LVF in the range of 0.0625–1 mM (Fig. 3c). The removal efficiency of LVF increased from 79.23% to nearly 100%, and the corresponding k_{obs} increased from 0.0518 to 0.2029 min^{-1} (Fig. S4).

3.2.2.2. Impact of inorganic anions and humic acid. In the $CoFe_2O_4$/PMS system, anions such as Cl^-, $H_2PO_4^-$, HCO_3^-, etc., will not only react with the active oxide species to produce radicals with weaker oxidation

capacity, but also will compete with PMS for the active binding sites on the surface of the $CoFe_2O_4$ NPs [40]. As shown in Fig. 4a, the removal efficiency of LVF was 94.66, 82.92%, 87.61%, and 89.15% when the concentrations of Cl^- was 0, 2, 10, and 50 mM, respectively, and the corresponding k_{obs} value was 0.0997, 0.0606, 0.0703, and 0.0750 min^{-1} (Fig.S5). Studies have been confirmed that Cl^- not only can react with $SO_4^{\bullet-}$ and HO• to generate less reactive chlorine radicals (Eqs. (9)–(18)) [53–57], but also can decompose PMS into $SO_4^{\bullet-}$ directly (Eq. (19)). The research results are consistent with previous studies [58,59]. However, the removal efficiencies of LVF were higher in the presence of 10 mM and 20 mM Cl^- compared with 5 mM Cl^-, which might be attributed to the large amount of $Cl^{\bullet}$ and $Cl_2^{\bullet-}$ production.

The removal efficiency of LVF was 94.66%, 37.80%, 33.84%, and 27.38% when 0, 5, 10, and 20 mM HCO_3^- were added into the reaction solution, respectively (Fig. 4b). Furthermore, the k_{obs} value decreased from 0.0997 min^{-1} to 0.00958 min^{-1} as the HCO_3^- dose increased (Fig. S5). HCO_3^- and CO_3^{2-} will be competed with LVF for $SO_4^{\bullet-}$ and HO• to produce less oxidizing $CO_3^{\bullet-}$ and $HCO_3^{\bullet-}$ (Eqs. (20) and (21)) [60,61] and can decompose PMS directly (Eq. (22)).

As shown in Fig. 4c, the removal efficiency of LVF was increased from 94.66% to nearly 100%, and the corresponding k_{obs} value was increased from 0.117 min^{-1} to 0.2152 min^{-1} (Fig. S5), when the concentration of $H_2PO_4^-$ increased from 0 mM to 5 mM. This result can be explained by the activation of PMS by low concentration of $H_2PO_4^-$ [62].

Natural organic matter (NOM) has abundant functional groups, such as carboxylic acid groups and phenolic groups etc., which may affect the AOPs process that base on $SO_4^{\bullet-}$ [63,64]. The addition of humic acid (HA) did not affect the final removal efficiency of LVF significantly, but the k_{obs} value increased from 0.0997 min^{-1} to 0.1126 min^{-1} as the HA concentration increased from 0 mg/L to 1 mg/L, and then decreased to 0.1011 min^{-1} and 0.0854 min^{-1} as the concentration of HA increased to 3 mg/L and 5 mg/L, respectively (Fig. S6). A similar phenomenon was observed during the degradation of sulfamethoxazole in the $CoFe_2O_4$-EG/PMS system [65]. Although the hydroquinone, quinones and phenols in HA could activate PMS to degrade the contaminant [66], excess HA may compete with LVF for the active species to affect the degradation efficiency of LVF. Meanwhile, HA will adsorb on the catalyst surface and result in the decrease of active sites number, or hinder the interaction between catalyst and PMS/LVF, and thereby reducing the removal efficiency of LVF [2,67].

$$SO_4^{\bullet-} + Cl^- \rightarrow SO_4^{2-}\cdot + Cl^{\bullet} \quad (k = (3.2 \pm 0.2) \times 10^8 M^{-1}s^{-1}) \tag{9}$$

$$HO\bullet + Cl^- \rightarrow Cl^{\bullet} + OH^- \quad (k = 4.3 \times 10^9\text{-}1.8 \times 10^{10} M^{-1}s^{-1}) \tag{10}$$

$$Cl^- + Cl^{\bullet} \rightarrow Cl_2^{\bullet-} \quad (k = 6.5 \times 10^9\text{-}2.1 \times 10^{10} M^{-1}s^{-1}) \tag{11}$$

$$H_2O + Cl_2^{\bullet-} \rightarrow ClOH^{\bullet-} + Cl^- + H^+ \quad (k = 24\ M^{-1}s^{-1}) \tag{12}$$

$$ClOH^{\bullet-} + Cl^- \rightarrow Cl_2^{\bullet-} + HO^- \quad (k = 10^5\ \ M^{-1}s^{-1}) \tag{13}$$

$$ClOH^{\bullet-} \rightarrow Cl^- + HO\bullet \quad (k = 6.1 \times 10^9 M^{-1}s^{-1}) \tag{14}$$

$$Cl_2^{\bullet-} + HO\bullet \rightarrow Cl^- + HOCl \quad (k = 1.0 \times 10^9 M^{-1}s^{-1}) \tag{15}$$

$$Cl_2^{\bullet-} \rightarrow Cl^- + Cl^{\bullet} \quad (k = 1.1 \times 10^5 M^{-1}s^{-1}) \tag{16}$$

$$Cl_2^{\bullet-} + Cl_2^{\bullet-} \rightarrow 2Cl^- + Cl_2 \quad (k = 6.3 \times 10^8 M^{-1}s^{-1}) \tag{17}$$

$$HSO_5^- + 2Cl^- + H^+ \rightarrow Cl_2 + SO_4^{2-} + H_2O \tag{18}$$

$$HSO_5^- + Cl^- \rightarrow SO_4^{2-} + HOCl \tag{19}$$

$$HO\bullet + CO_3^{2} \dashrightarrow OH\text{-} + CO_3^{\bullet-} \quad (k = 8.5 \times 10^6 M^{-1}s^{-1}) \tag{20}$$

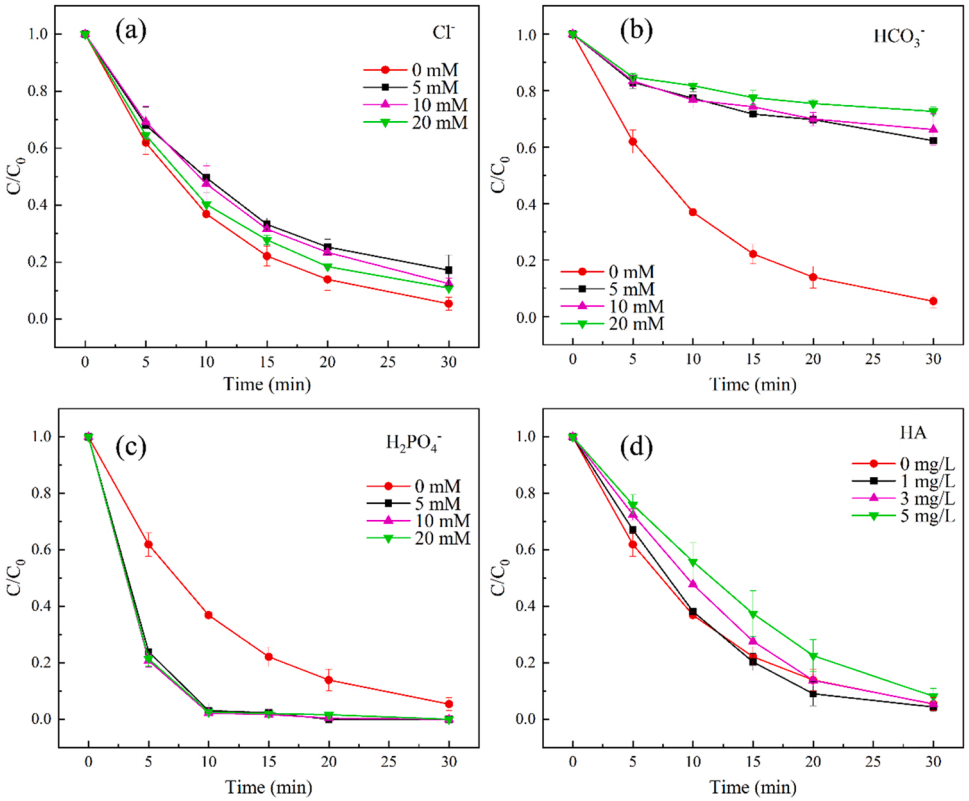

Fig. 4. Effect of Cl^- (a), HCO_3^- (b), $H_2PO_4^-$ (c), and HA on LVF degradation (reaction conditions: $[CoFe_2O_4]$=100 mg/L, [PMS]=0.25 mM, [LVF]=5 mg/L, pH_0 =7, T = 25 °C).

$$SO4\bullet- + HCO3- \rightarrow HCO3\bullet + SO_4^{2-} \quad (k = 1.6 \times 10^6 M^{-1}s^{-1}) \quad (21)$$

$$HSO_5^- + HCO_3^- \rightarrow HSO_4^- + HCO4- \quad (22)$$

3.3. Identification of reactive species

The radical-based ($SO_4^{\bullet-}$ and HO•) oxidation pathway was considered to be the key mechanism for organic pollutants removal in $CoFe_2O_4$/PMS system, irrespective of the negligible contribution of direct PMS oxidation and $CoFe_2O_4$ NPs adsorption effect [31,38,46,68]. Therefore, ethanol (EtOH) and tert-butanol (TBA) were used to distinguish the contribution of $SO_4^{\bullet-}$ and HO•. Generally, TBA is an effective HO• scavenger [69] and EtOH can be used to quench both $SO_4^{\bullet-}$ and HO•, since the reaction rate of TBA with HO• is 1000 times faster than that with $SO_4^{\bullet-}$ (Eqs. (23) and (24)) [70], while the reaction rate of EtOH with the above two radicals is similar (Eqs. (25) and (26)) [71]. As shown in Fig. 5, the removal efficiency of LVF slightly decreased from 96.67% to 96.08% and 96.21%, respectively, with the addition of 50 mM and 100 mM TBA to the reaction solution, and the corresponding k_{obs} value decreased from 0.1118 min^{-1} to 0.1038 min^{-1} and 0.1048 min^{-1}. The results indicated weak contribution of HO• to LVF removal. However, when 50 mM and 100 mM EtOH was added, the removal efficiency of LVF decreased from 96.67% to 55.59% and 43.42%, respectively, and the corresponding k_{obs} value was decreased from 0.1118 min^{-1} to 0.0261 min^{-1} and 0.0178 min^{-1} (Fig. S7). When the $[Quencher]_0/[PMS]_0$ ratio was 100 and 200, the contribution of HO• was 0.61% and 0.48%, and the contribution of $SO_4^{\bullet-}$ was 41.88% and 54.61% (Table S1). Therefore, $SO_4^{\bullet-}$ played a dominant role in the degradation of LVF in $CoFe_2O_4$/PMS system.

$$SO4\bullet- + TBA \rightarrow \text{intermediates} \quad k_1 = (4\text{-}9.1) \times 10^5 M^{-1} \quad s^{-1} \quad (23)$$

$$HO\bullet + TBA \rightarrow \text{intermediates} \quad k_2 = (3.8\text{-}7.6) \times 10^8 M^{-1} \quad s^{-1} \quad (24)$$

$$SO4\bullet- + EtOH \rightarrow \text{intermediates} \quad k_3 = (1.6\text{-}7.7) \times 10^7 M^{-1} \quad s^{-1} \quad (25)$$

$$HO\bullet + EtOH \rightarrow \text{intermediates} \quad k_4 = (1.2\text{-}2.8) \times 10^9 M^{-1} \quad s^{-1} \quad (26)$$

The EPR experiments using DMPO as the spin-trapping agent are performed to identify the main radical species in the PMS alone and $CoFe_2O_4$/PMS experiment, and the EPR spectra are shown in Fig. S8. No signals were obtained in the PMS alone experiment, while DMPO-SO_4 and DMPO-OH signals were clearly identified in $CoFe_2O_4$/PMS experiment with the splitting of 1:2:2:1 and 1:1:1:1:1:1 characteristic peak [22], respectively. The results were further confirmed that $SO_4^{\bullet-}$ and HO• are the main radical species in $CoFe_2O_4$/PMS system.

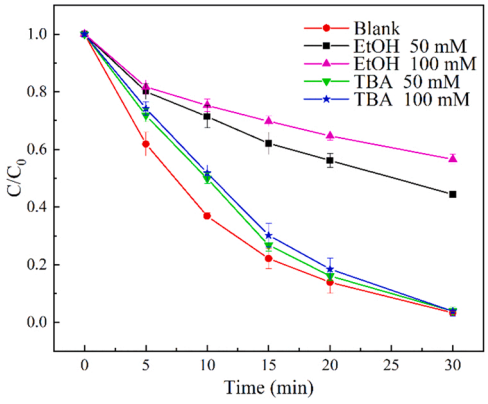

Fig. 5. The effect of radical scavengers on LVF degradation (reaction conditions: $[CoFe_2O_4]$ =100 mg/L, [PMS]=0.25 mM, [LVF]=5 mg/L, pH_0 =7, T = 25 °C).

3.4. Mechanism of LVF degradation and the proposed degradation pathways

3.4.1. Mechanisms of PMS activation

XPS analysis was performed to determine the surface electronic states and chemical composition of the $CoFe_2O_4$ NPs before and after reaction (Fig. 6). The full-scale XPS spectrums were corrected by C 1 s peak (284.8 eV, Fig. 6a). As shown in Fig. 6b, three peaks were observed in fresh $CoFe_2O_4$ NPs at Co $2p_{3/2}$ (780.2 eV, 782.5 eV) and Co $2p_{1/2}$ (795.9 eV), which is assigned to ≡Co(II) at the octahedral site (B-site), ≡Co(II) at the tetrahedral site (A-site), and ≡Co(III) [16,64]. ≡Co(II) and ≡Co(III) accounted for 69.9% and 30.1% before the reaction, and change into 58.3% and 41.7% after the reaction. As shown in XPS spectrum of Fe 2p (Fig. 6c), the peaks at 710.5 eV and 712.7 eV are ascribed to ≡Fe(II) and ≡Fe(III), respectively [16], and the relative area ratio of the two peaks was 43.6% and 56.4% in fresh $CoFe_2O_4$, while changed into 50.9% and 49.1% after the reaction. In view of the reduction potentials of $HSO_5^-/SO_4\bullet-$ (2.5–3.1 V) and $HSO_5^-/SO_5\bullet-$ (1.1 V) [72], the ≡Co(III)/≡Co(II) redox cycle is thermodynamically feasible due to the appropriate reduction potential (1.81 V). While the regeneration of ≡Fe(II) is thermodynamically unfavorable [73]. Therefore, it can be proposed that both surface ≡Co(II)/≡Co(III) and ≡Fe(II)/≡Fe(III) redox pairs are involved in PMS catalysis, and ≡Co(II)/≡Co(III) redox pairs play a dominant role. In addition, the regeneration of ≡Co(II) is mainly depended on the reaction with PMS (Eq. (27)) [40], thus result in significantly increase of ≡Co(III) percentage in the condition of small amount of PMS dosage.

$$\equiv o^{3+} + HSO_5^- \rightarrow \equiv o^{2+} + SO_5^{2-} + H_2O \quad (27)$$

In the O1s spectra, the dominant peak centered around 529.9 eV (Fig. 6d) belonged to the typical lattice oxygen in metal oxides (MO−), and the peak at 531.6 eV was attributed to the hydroxyl component on the surface of $CoFe_2O_4$ NPs [37]. The relative content of lattice oxygen decreased from 64.2% to 54.0%, while the surface hydroxyl component (531.6 eV, −OH) increased from 35.8% to 46%. The ratio of the −OH/MO− increase from 0.56 to 0.85 suggests the generation of M-OH groups on the catalyst surface $CoFe_2O_4$ NPs [74], and also indicates the oxidation of surface M(II) to M(III) for PMS activation [45].

3.4.2. Proposed degradation pathways of LVF and toxicity estimation

Although the removal efficiency of LVF can be reached 95.4% in $CoFe_2O_4$/PMS system, the TOC removal efficiency was just about 27.0% (Fig. S9). The structures of the degradation products (Table S2) were determined based on the fragmentation patterns obtained from UPLC-MS analysis and information from previous literature. Five degradation pathways were proposed base on the identified eleven degradation products, including demethylation, defluorination, decarboxylation, transformations of piperazine ring and conversion of quinolone moieties (Fig. 7).

(1) Demethylation

P1 (*m/z* 348) in pathway A can be attributed to the demethylation of the piperazine ring and the addition of hydrogen atoms [75], which has been also detected during the photocatalytic degradation of LVF [76]. P2 (*m/z* 392) is the carboxylated products of LVF, and then P3 (*m/z* 348) was generated by decarboxylation reaction [77].

(2) Defluorination

In pathway B, P4 (*m/z* 360) will be generated by defluorination reaction, which has been identified as the degradation product of LVF in the $ZnFe_2O_4$/PMS system [75] and the oxidative degradation of LVF by permanganate [78].

(3) Decarboxylation

P6 (*m/z* 318) in degradation pathway C is the decarboxylation product. The decarboxylation reaction is a common pathway for

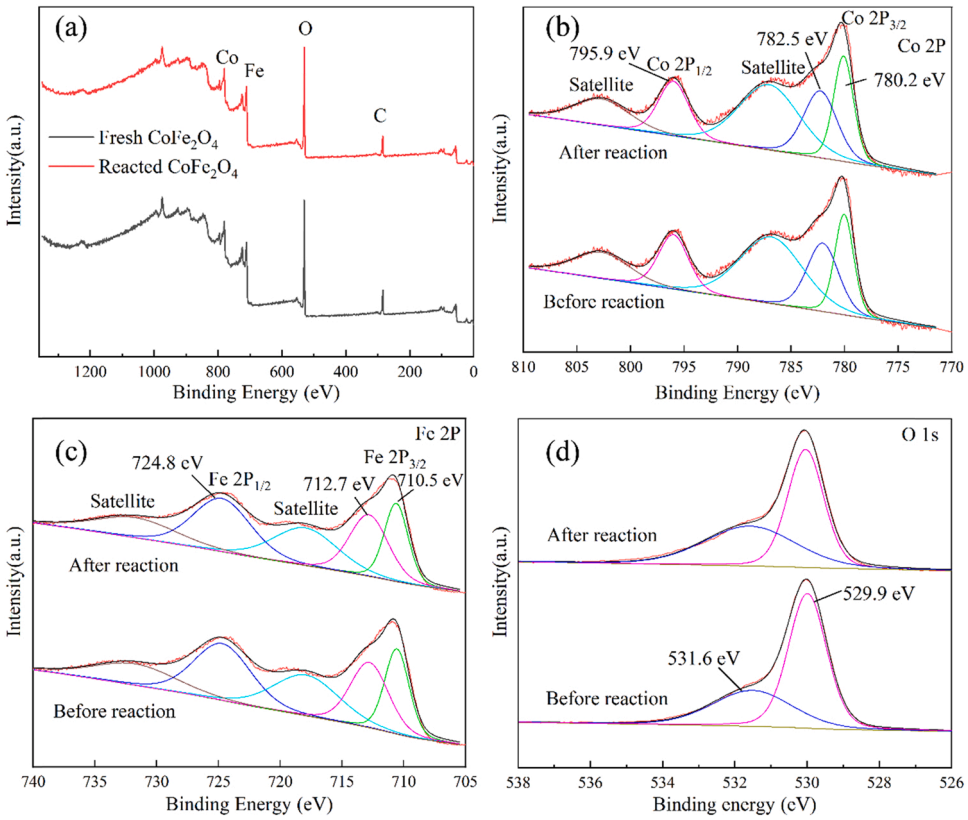

Fig. 6. The XPS spectra of whole survey (a) and Co 2p (b), Fe 2p (c), and O 1s (d) of $CoFe_2O_4$ NPs before and after reaction.

the self-sensitized oxidation of fluoroquinolones (FQs) via HO• [79,80], and also detected during the degradation of LVF using $Ag_2CO_3/CeO_2/AgBr$ as photocatalyst under visible light irradiation [77]. It is the first time that the dehydroxylation product P5 (*m/z* 346) was detected in heterogeneous catalytic oxidation reaction.

(4) Transformations of piperazine ring

The oxidation of piperazine ring is considered as the one of the main conversion pathways of FQs in AOPs [81]. In degradation pathway D, LVF was decomposed through de-piperazinylation to generate P7 (*m/z* 336), which would be further decomposed to P8 (*m/z* 322) and P9 (*m/z* 264). Similar degradation pathway is obtained in photocatalytic degradation of LVF [82], but the deep oxidation products (liberation of the F-groups accompanied by decarboxylation) have not been obtained in this study.

(5) Conversion of quinolone moieties

The conversion of quinolone molecules is another major pathway for free radicals to attack LVF [81]. In pathway E, it can be assumed that P10 (*m/z* 394) is the reaction product of the reactive radical attack on the quinolone moiety [75], which will be further oxidized by $SO_4^{\bullet-}$ to produce P11 (*m/z* 338).

3.5. Toxicity estimation of LVF and its degradation products

The calculated LC_{50}, EC_{50}, and ChV value of LVF and its degradation products were listed in Table S3. The acute toxicity was expressed as LC_{50} (fish and Daphnia) and EC_{50} (green algae), and the chronic toxicity was expressed as ChV (fish, Daphnia and green algae). The results indicated that the degradation product P5, P6 (pathway C), and P11 (pathway E) showed lower acute toxicity values and chronic toxicity values compared with LVF, suggesting a higher risk. Especially, the acute toxicity of P6 and P11 to Daphnia and green algae, and the chronic toxicity to Daphnia increased from not harmful to toxic. However, there were no very toxic degradation products generated during the reaction ($LC_{50}/EC_{50} \leq 1$ or ChV<0.1). It can be assumed that, although $SO_4^{\bullet-}$ was the dominant free radical in $CoFe_2O_4$/PMS system, the deep oxidative degradation of LVF is difficult. Meanwhile, the existence of HO• in the $CoFe_2O_4$/PMS system would inevitably result in the self-sensitized oxidation of FQs. Therefore, in order to avoid the production of highly toxic products or achieve their deep oxidation needs further research via the target optimization of $CoFe_2O_4$/PMS system, including the PMS replenish at a specific reaction stage, inhibits hydroxyl radical formation, or conjunction with other auxiliary means.

In addition, the toxicity tests were performed based on the photobacterium phosphoreum to investigated the environmental impact of LVF and its degradation intermediates. As shown in Fig. 8, the luminescence inhibition ratio of the reaction solution significantly increased from 21.4% to 46.5% after 5 min in $CoFe_2O_4$/PMS system, and slightly increased to 49.0% after the next 5 min, while the value was finally decreased to 23.5% by the end of the experiment. The results were consistent with the degradation trends of LVF. The rapid decomposition of LVF during the first 10 min in $CoFe_2O_4$/PMS system has resulted in the accumulation of degradation intermediates, especially the degradation product P5 and P11, which would be generated first in the degradation pathway C and pathway B, respectively. Meanwhile, P6 was produced by the further degradation of P5, which might be existed in a certain amount in $CoFe_2O_4$/PMS system by the end of the experiment, thus the luminescence inhibition ratio was still higher than the original LVF solution. Therefore, in order to eliminate the environmental impact of LVF and its degradation intermediates, the degradation pathways that generate toxic products should be avoided or detoxification by the complete mineralization of LVF, which needs further research via the targeted optimization of $CoFe_2O_4$/PMS system.

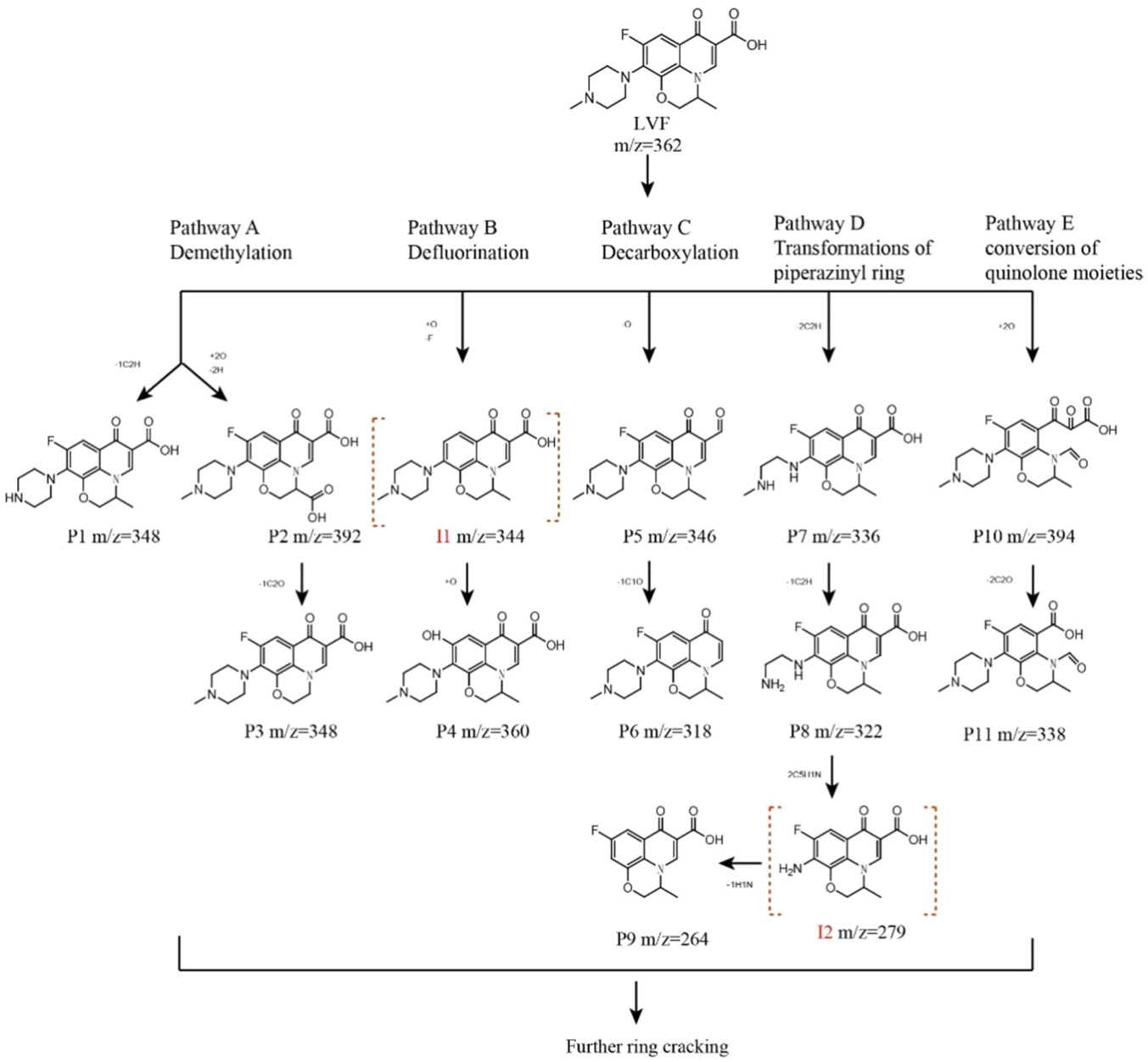

Fig. 7. Proposed degradation pathways of LVF in $CoFe_2O_4$/PMS system.

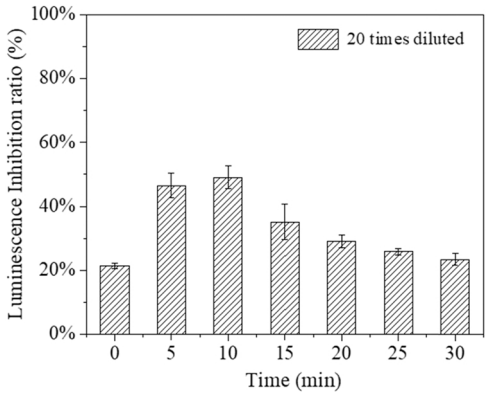

Fig. 8. Change in effluent toxicity during the degradation of LVF in $CoFe_2O_4$/PMS system.

4. Conclusion

In this study, $CoFe_2O_4$ NPs were successfully synthesized and exhibited excellent PMS catalytic performance to degrade LVS. The removal efficiency of LVF increased with the dosage of PMS and $CoFe_2O_4$ NPs, and did not show significant difference in the condition of pH= 5–9 with the same other reaction parameters, but significantly decreased under extremely alkaline (pH=11) and acidic (pH=3) condition. The removal efficiency of LVF (initial concentration was 5 mg/L) could be reached 95.4% under the optimal reaction conditions (pH_0 =7, $CoFe_2O_4$ NPs dosage=100 mg/L, PMS dosage=0.25 mM). Both $SO_4^{\bullet-}$ and HO• were involved in the degradation of LVF, but $SO_4^{\bullet-}$ played a decisive role in $CoFe_2O_4$/PMS system. The presence HCO_3^- would be significantly inhibited the degradation of LVF, while $H_2PO_4^-$ showed a strong degradation promoting effect. However, the LVF degradation inhibitory effect would be decreased as Cl^- concentration increased, while increased with the humic acid concentration. Five possible degradation pathways of LVF were proposed based on the eleven

detected degradation products, including demethylation, defluorination, decarboxylation, conversion of the piperazine ring and conversion of quinolone molecules (CQM). The toxicity estimation results indicated that the degradation product P5, P6 and P11, which were generated in the degradation pathway of decarboxylation (P5 and P6) and CQM (P11), showed higher acute and chronic toxicity compared with LVF. The coexistence of $SO_4^{\bullet-}$ and HO• in $CoFe_2O_4$/PMS system were the reasons for the generation of high toxic degradation products. Although no very toxic degradation products were generated during the reaction, the methods to avoid the generation of toxic products or achieve deep oxidation of LVF still needs further research.

CRediT authorship contribution statement

Lili Liu: Methodology, Writing – original draft, Validation. **Rui Zhan:** Software, Investigation. **Meng Zhang:** Conceptualization, Writing – review & editing, Validation. **Jianan Li:** Investigation, Software, Formal analysis. **Zhiping Wang:** Supervision, Writing – review & editing. **Haosheng Mi:** Investigation, Software. **Yunxiao Zhang:** Investigation.

Declaration of Competing Interest

The authors declare that they have no known competing financial interests or personal relationships that could have appeared to influence the work reported in this paper.

Acknowledgments

This work was supported by National Natural Science Foundation of China (Grant No. 41771513, 41907110), China Postdoctoral Science Foundation (Grant No. 2020M671029), and National Key Research and Development Program of China (Grant No. 2018YFC1901000).

Appendix A. Supporting information

Supplementary data associated with this article can be found in the online version at doi:10.1016/j.jece.2022.107435.

References

[1] S. Babić, M. Periša, I. Škorić, Photolytic degradation of norfloxacin, enrofloxacin and ciprofloxacin in various aqueous media, Chemosphere 91 (2013) 1635–1642, https://doi.org/10.1016/j.chemosphere.2012.12.072.
[2] L. Chen, D. Ding, C. Liu, H. Cai, Y. Qu, S. Yang, Y. Gao, T. Cai, Degradation of norfloxacin by $CoFe_2O_4$-GO composite coupled with peroxymonosulfate: a comparative study and mechanistic consideration, Chem. Eng. J. 334 (2018) 273–284, https://doi.org/10.1016/j.cej.2017.10.040.
[3] Y. Wang, D. Tian, W. Chu, M. Li, X. Lu, Nanoscaled magnetic $CuFe_2O_4$ as an activator of peroxymonosulfate for the degradation of antibiotics norfloxacin, Sep. Purif. Technol. 212 (2019) 536–544, https://doi.org/10.1016/j.seppur.2018.11.051.
[4] M.L. Devi, K. Chandrasekhar, A validated stability-indicating RP-HPLC method for levofloxacin in the presence of degradation products, its process related impurities and identification of oxidative degradant, J. Pharm. Biomed. Anal. 50 (2009) 710–717, https://doi.org/10.1016/j.jpba.2009.05.038.
[5] L. Riaz, T. Mahmood, A. Kamal, M. Shafqat, A. Rashid, Industrial release of fluoroquinolones (FQs) in the waste water bodies with their associated ecological risk in Pakistan, Environ. Toxicol. Pharm. 52 (2017) 14–20, https://doi.org/10.1016/j.etap.2017.03.002.
[6] Z. Li, M. Li, Z. Zhang, P. Li, Y. Zang, X. Liu, Antibiotics in aquatic environments of China: a review and meta-analysis, Ecotoxicol. Environ. Saf. 199 (2020), 110668, https://doi.org/10.1016/j.ecoenv.2020.110668.
[7] L. Riaz, T. Mahmood, A. Khalid, A. Rashid, M.B.A. Siddique, A. Kamal, M.S. Coyne, Fluoroquinolones (FQs) in the environment: a review on their abundance, sorption and toxicity in soil, Chemosphere 191 (2018) 704–720, https://doi.org/10.1016/j.chemosphere.2017.10.092.
[8] F. Ay, F. Kargi, Advanced oxidation of amoxicillin by Fenton's reagent treatment, J. Hazard. Mater. 179 (2010) 622–627, https://doi.org/10.1016/j.jhazmat.2010.03.048.
[9] M. Cheng, G. Zeng, D. Huang, C. Lai, Y. Liu, C. Zhang, J. Wan, L. Hu, C. Zhou, W. Xiong, Efficient degradation of sulfamethazine in simulated and real wastewater at slightly basic pH values using Co-SAM-SCS /H_2O_2 Fenton-like system, Water Res. 138 (2018) 7–18, https://doi.org/10.1016/j.watres.2018.03.022.
[10] I. Epold, M. Trapido, N. Dulova, Degradation of levofloxacin in aqueous solutions by Fenton, ferrous ion-activated persulfate and combined Fenton/persulfate systems, Chem. Eng. J. 279 (2015) 452–462, https://doi.org/10.1016/j.cej.2015.05.054.
[11] S. Zha, Y. Cheng, Y. Gao, Z. Chen, M. Megharaj, R. Naidu, Nanoscale zero-valent iron as a catalyst for heterogeneous Fenton oxidation of amoxicillin, Chem. Eng. J. 255 (2014) 141–148, https://doi.org/10.1016/j.cej.2014.06.057.
[12] M.G. Antoniou, A. Armah, D.D. Dionysiou, Degradation of microcystin-LR using sulfate radicals generated through photolysis, thermolysis and e^- transfer mechanisms, Appl. Catal. B Environ. 96 (2010) 290–298, https://doi.org/10.1016/j.apcatb.2010.02.013.
[13] P. Neta, R.E. Huie, A.B. Ross, Rate constants for reactions of inorganic radicals in aqueous solution, J. Phys. Chem. Ref. Data 17 (1988) 1027–1284, https://doi.org/10.1063/1.555808.
[14] T. Olmez-Hanci, I. Arslan-Alaton, Comparison of sulfate and hydroxyl radical based advanced oxidation of phenol, Chem. Eng. J. 224 (2013) 10–16, https://doi.org/10.1016/j.cej.2012.11.007.
[15] R. Yuan, S.N. Ramjaun, Z. Wang, J. Liu, Effects of chloride ion on degradation of Acid Orange 7 by sulfate radical-based advanced oxidation process: implications for formation of chlorinated aromatic compounds, J. Hazard. Mater. 196 (2011) 173–179, https://doi.org/10.1016/j.jhazmat.2011.09.007.
[16] C. Cai, S. Kang, X. Xie, C. Liao, X. Duan, D.D. Dionysiou, Efficient degradation of bisphenol A in water by heterogeneous activation of peroxymonosulfate using highly active cobalt ferrite nanoparticles, J. Hazard. Mater. 399 (2020), 122979, https://doi.org/10.1016/j.jhazmat.2020.122979.
[17] Y.H. Li, W.J. Zhu, Q. Guo, X. Wang, L.M. Zhang, X.Y. Gao, Y.M. Luo, Highly efficient degradation of sulfamethoxazole (SMX) by activating peroxymonosulfate (PMS) with $CoFe_2O_4$ in a wide pH range, Sep. Purif. Technol. 276 (2021), 119403, https://doi.org/10.1016/j.seppur.2021.119403.
[18] H.D. Chen, J.K. Xu, J.Q. Wei, P.F. Wang, Y.B. Han, J.C. Xu, B. Hong, H.X. Jin, D. F. Jin, X.L. Peng, J. Li, Y.T. Yang, H.L. Ge, X.Q. Wang, Mesoporous $CoFe_2O_4$ nanowires: nanocasting synthesis, magnetic separation and enhanced catalytic degradation for ciprofloxacin, J. Phys. Chem. Solids 132 (2019) 138–144, https://doi.org/10.1016/j.jpcs.2019.04.008.
[19] L.L. Liu, H.S. Mi, M. Zhang, F.F. Sun, R. Zhan, H.B. Zhao, S.Q. He, L. Zhou, Efficient moxifloxacin degradation by $CoFe_2O_4$ magnetic nanoparticles activated peroxymonosulfate: kinetics, pathways and mechanisms, Chem. Eng. J. 407 (2020), 127201, https://doi.org/10.1016/j.cej.2020.127201.
[20] Y. Fan, Y.R. Liu, X. Hu, Z.R. Sun, Preparation of metal organic framework derived materials $CoFe_2O_4$@NC and its application for degradation of norfloxacin from aqueous solutions by activated peroxymonosulfate, Chemosphere 275 (2021), 130059, https://doi.org/10.1016/j.chemosphere.2021.130059.
[21] J.Y. Liu, R. Meng, J.X. Li, P.M. Jian, L.X. Wang, R.Q. Jian, Achieving high-performance for catalytic epoxidation of styrene with uniform magnetically separable $CoFe_2O_4$ nanoparticles, Appl. Catal. B Environ. 254 (2019) 214–222, https://doi.org/10.1016/j.apcatb.2019.04.083.
[22] X. Li, Z.H. Wang, B. Zhang, A.I. Rykov, M.A. Ahmed, J.H. Wang, $FexCo_{3-x}O_4$ nanocages derived from nanoscale metalorganic frameworks for removal of bisphenol A by activation of peroxymonosulfate, Appl. Catal. B Environ. 181 (2016) 788–799, https://doi.org/10.1016/j.apcatb.2015.08.05.
[23] G.P. Anipsitakis, D.D. Dionysiou, Degradation of organic contaminants in water with sulfate radicals generated by the conjunction of peroxymonosulfate with cobalt, Environ. Sci. Technol. 37 (2003) 4790–4797, https://doi.org/10.1021/es0263792.
[24] J. Wang, B. Xiong, L. Miao, S. Wang, P. Xie, Z. Wang, J. Ma, Applying a novel advanced oxidation process of activated peracetic acid by $CoFe_2O_4$ to efficiently degrade sulfamethoxazole, Appl. Catal. B Environ. 280 (2021), 119422, https://doi.org/10.1016/j.apcatb.2020.119422.
[25] Y. Gao, D. Zou, Efficient degradation of levofloxacin by a microwave–3D $ZnCo_2O_4$/activated persulfate process: effects, degradation intermediates, and acute toxicity, Chem. Eng. J. 393 (2020), 124795, https://doi.org/10.1016/j.cej.2020.124795.
[26] F. Meng, Y. Wang, Z. Chen, J. Hu, G. Lu, W. Ma, Synthesis of CQDs@ FeOOH nanoneedles with abundant active edges for efficient electro-catalytic degradation of levofloxacin: degradation mechanism and toxicity assessment, Appl. Catal. B Environ. 282 (2021), 119597, https://doi.org/10.1016/j.apcatb.2020.119597.
[27] W. Chen, X. Li, Z. Pan, S. Ma, L. Li, Synthesis of MnOx/SBA-15 for Norfloxacin degradation by catalytic ozonation, Sep. Purif. Technol. 173 (2017) 99–104, https://doi.org/10.1016/j.seppur.2016.09.030.
[28] K. Yin, L. Deng, J. Luo, J. Crittenden, C. Liu, Y. Wei, L. Wang, Destruction of phenicol antibiotics using the UV/H_2O_2 process: kinetics, byproducts, toxicity evaluation and trichloromethane formation potential, Chem. Eng. J. 351 (2018) 867–877, https://doi.org/10.1016/j.cej.2018.06.164.
[29] M. Feng, Z. Wang, D.D. Dionysiou, V.K. Sharma, Metal-mediated oxidation of fluoroquinolone antibiotics in water: a review on kinetics, transformation products, and toxicity assessment, J. Hazard. Mater. 344 (2018) 1136–1154, https://doi.org/10.1016/j.jhazmat.2017.08.067.
[30] Y. Ji, C. Ferronato, A. Salvador, X. Yang, J.-M. Chovelon, Degradation of ciprofloxacin and sulfamethoxazole by ferrous-activated persulfate: implications for remediation of groundwater contaminated by antibiotics, Sci. Total Environ. 472 (2014) 800–808, https://doi.org/10.1016/j.scitotenv.2013.11.008.
[31] Y. Ren, L. Lin, J. Ma, J. Yang, J. Feng, Z. Fan, Sulfate radicals induced from peroxymonosulfate by magnetic ferrospinel MFe_2O_4 (M=Co, Cu, Mn, and Zn) as heterogeneous catalysts in the water, Appl. Catal. B Environ. 165 (2015) 572–578, https://doi.org/10.1016/j.apcatb.2014.10.051.

[32] Y. Gao, Y. Ji, G. Li, T. An, Theoretical investigation on the kinetics and mechanisms of hydroxyl radical-induced transformation of parabens and its consequences for toxicity: Influence of alkyl-chain length, Water Res. 91 (2016) 77–85, https://doi.org/10.1016/j.watres.2015.12.056.
[33] X. Li, X. Liu, C. Lin, H. Zhang, Z. Zhou, G. Fan, J. Ma, Cobalt ferrite nanoparticles supported on drinking water treatment residuals: an efficient magnetic heterogeneous catalyst to activate peroxymonosulfate for the degradation of atrazine, Chem. Eng. J. 367 (2019) 208–218, https://doi.org/10.1016/j.cej.2019.02.151.
[34] K.-Y.A. Lin, M.-T. Yang, J.-T. Lin, Y. Du, Cobalt ferrite nanoparticles supported on electrospun carbon fiber as a magnetic heterogeneous catalyst for activating peroxymonosulfate, Chemosphere 208 (2018) 502–511, https://doi.org/10.1016/j.chemosphere.2018.05.127.
[35] D. Ding, Y. Huang, C. Zhou, Z. Liu, J. Ren, R. Zhang, J. Wang, Y. Zhang, Z. Lei, Z. Zhang, Facet-controlling agents free synthesis of hematite crystals with high-index planes: excellent photodegradation performance and mechanism insight, ACS Appl. Mater. Interfaces 8 (2016) 142–151, https://doi.org/10.1021/acsami.5b07843.
[36] P. Hong, Y. Li, J. He, A. Saeed, K. Zhang, C. Wang, L. Kong, J. Liu, Rapid degradation of aqueous doxycycline by surface $CoFe_2O_4/H_2O_2$ system: behaviors, mechanisms, pathways and DFT calculation, Appl. Surf. Sci. 526 (2020), 146557, https://doi.org/10.1016/j.apsusc.2020.146557.
[37] L. Chen, X. Zuo, L. Zhou, Y. Huang, S. Yang, T. Cai, D. Ding, Efficient heterogeneous activation of peroxymonosulfate by facilely prepared Co/Fe bimetallic oxides: kinetics and mechanism, Chem. Eng. J. 345 (2018) 364–374, https://doi.org/10.1016/j.cej.2018.03.169.
[38] Q. Song, Y. Feng, Z. Wang, G. Liu, W. Lv, Degradation of triphenyl phosphate (TPhP) by $CoFe_2O_4$-activated peroxymonosulfate oxidation process: kinetics, pathways, and mechanisms, Sci. Total Environ. 681 (2019) 331–338, https://doi.org/10.1016/j.scitotenv.2019.05.105.
[39] H. Chun, W. Yizhong, T. Hongxiao, Preparation and characterization of surface bond-conjugated TiO_2/SiO_2 and photocatalysis for azo dyes, Appl. Catal. B Environ. 30 (2001) 277–285, https://doi.org/10.1016/S0926-3373(00)00237-X.
[40] C. Liang, Z.-S. Wang, C.J. Bruell, Influence of pH on persulfate oxidation of TCE at ambient temperatures, Chemosphere 66 (2007) 106–113, https://doi.org/10.1016/j.chemosphere.2006.05.026.
[41] Q. Wang, Y. Shao, N. Gao, W. Chu, J. Chen, X. Lu, Y. Zhu, N. An, Activation of peroxymonosulfate by Al_2O_3-based $CoFe_2O_4$ for the degradation of sulfachloropyridazine sodium: kinetics and mechanism, Sep. Purif. Technol. 189 (2017) 176–185, https://doi.org/10.1016/j.seppur.2017.07.046.
[42] Y. Zhu, S. Chen, X. Quan, Y. Zhang, Cobalt implanted TiO_2 nanocatalyst for heterogeneous activation of peroxymonosulfate, RSC Adv. 3 (2013) 520–525, https://doi.org/10.1016/10.1039/C2RA22039C.
[43] A.A. Isari, S. Moradi, S.S. Rezaei, F. Ghanbari, E. Dehghanifard, B. Kakavandi, Peroxymonosulfate catalyzed by core/shell magnetic ZnO photocatalyst towards degradation of malathion: enhancing synergy, catalytic performance and mechanism, Sep. Purif. Technol. 275 (2021), 119163, https://doi.org/10.1016/j.seppur.2021.119163.
[44] Y. Ji, C. Dong, D. Kong, J. Lu, Q. Zhou, Heat-activated persulfate oxidation of atrazine: implications for remediation of groundwater contaminated by herbicides, Chem. Eng. J. 263 (2015) 45–54, https://doi.org/10.1016/j.cej.2014.10.097.
[45] J. Di, M. Zhu, R. Jamakanga, X. Gai, Y. Li, R. Yang, Electrochemical activation combined with advanced oxidation on $NiCo_2O_4$ nanoarray electrode for decomposition of Rhodamine B, J. Water Process. Eng. 37 (2020), 101386, https://doi.org/10.1016/j.jwpe.2020.101386.
[46] Z. Wang, Y. Du, Y. Liu, B. Zou, J. Xiao, J. Ma, Degradation of organic pollutants by $NiFe_2O_4$/peroxymonosulfate: efficiency, influential factors and catalytic mechanism, RSC Adv. 6 (2016) 11040–11048, https://doi.org/10.1039/c5ra21117d.
[47] J. Deng, Y. Shao, N. Gao, C. Tan, S. Zhou, X. Hu, $CoFe_2O_4$ magnetic nanoparticles as a highly active heterogeneous catalyst of oxone for the degradation of diclofenac in water, J. Hazard. Mater. 262 (2013) 836–844, https://doi.org/10.1016/j.jhazmat.2013.09.049.
[48] Y. Du, W. Ma, P. Liu, B. Zou, J. Ma, Magnetic $CoFe_2O_4$ nanoparticles supported on titanate nanotubes ($CoFe_2O_4$/TNTs) as a novel heterogeneous catalyst for peroxymonosulfate activation and degradation of organic pollutants, J. Hazard. Mater. 308 (2016) 58–66, https://doi.org/10.1016/j.jhazmat.2016.01.035.
[49] N.H. El Najjar, A. Touffet, M. Deborde, R. Journel, N.K.V. Leitner, Levofloxacin oxidation by ozone and hydroxyl radicals: kinetic study, transformation products and toxicity, Chemosphere 93 (2013) 604–611, https://doi.org/10.1016/j.chemosphere.2013.05.086.
[50] S. Madihi-Bidgoli, S. Asadnezhad, A. Yaghoot-Nezhad, A. Hassani, Azurobine degradation using Fe_2O_3@ multi-walled carbon nanotube activated peroxymonosulfate (PMS) under UVA-LED irradiation: performance, mechanism and environmental application, J. Environ. Chem. Eng. 9 (2021), 106660, https://doi.org/10.1016/j.jece.2021.106660.
[51] F. Ghanbari, M. Khatebasreh, M. Mahdavianpour, A. Mashayekh-Salehi, E. Aghayani, K.Y.A. Lin, B.K. Noredinvand, Evaluation of peroxymonosulfate/O_3/UV process on a real polluted water with landfill leachate: feasibility and comparative study, Korean J. Chem. Eng. 38 (2021) 1416–1424, https://doi.org/10.1007/s11814-021-0782-8.
[52] C. Qi, X. Liu, J. Ma, C. Lin, X. Li, H. Zhang, Activation of peroxymonosulfate by base: Implications for the degradation of organic pollutants, Chemosphere 151 (2016) 280–288, https://doi.org/10.1016/j.chemosphere.2016.02.089.
[53] J. Li, M. Xu, G. Yao, B. Lai, Enhancement of the degradation of atrazine through $CoFe_2O_4$ activated peroxymonosulfate (PMS) process: kinetic, degradation intermediates, and toxicity evaluation, Chem. Eng. J. 348 (2018) 1012–1024, https://doi.org/10.1016/j.cej.2018.05.032.
[54] J. Deng, M. Xu, C. Qiu, Y. Chen, X. Ma, N. Gao, X. Li, Magnetic $MnFe_2O_4$ activated peroxymonosulfate processes for degradation of bisphenol A: performance, mechanism and application feasibility, Appl. Surf. Sci. 459 (2018) 138–147, https://doi.org/10.1016/j.apsusc.2018.07.198.
[55] Y. Huang, B. Sheng, Z. Wang, Q. Liu, R. Yuan, D. Xiao, J. Liu, Deciphering the degradation/chlorination mechanisms of maleic acid in the Fe(II)/peroxymonosulfate process: an often overlooked effect of chloride, Water Res. 145 (2018) 453–463, https://doi.org/10.1016/j.watres.2018.08.055.
[56] C. Tan, N. Gao, D. Fu, J. Deng, L. Deng, Efficient degradation of paracetamol with nanoscaled magnetic $CoFe_2O_4$ and $MnFe_2O_4$ as a heterogeneous catalyst of peroxymonosulfate, Sep. Purif. Technol. 175 (2017) 47–57, https://doi.org/10.1016/j.seppur.2016.11.016.
[57] B. Nikravesh, A. Shomalnasab, A. Nayyer, N. Aghababaei, R. Zarebi, F. Ghanbari, UV/Chlorine process for dye degradation in aqueous solution: mechanism, affecting factors and toxicity evaluation for textile wastewater, J. Environ. Chem. Eng. 8 (2020), 104244, https://doi.org/10.1016/j.jece.2020.104244.
[58] F. Ghanbari, M. Moradi, Application of peroxymonosulfate and its activation methods for degradation of environmental organic pollutants: review, Chem. Eng. J. 310 (2017) 41–62, https://doi.org/10.1016/j.cej.2016.10.064.
[59] J. Wang, S. Wang, Activation of persulfate (PS) and peroxymonosulfate (PMS) and application for the degradation of emerging contaminants, Chem. Eng. J. 334 (2018) 1502–1517, https://doi.org/10.1016/j.cej.2017.11.059.
[60] L. Liu, S. Lin, W. Zhang, U. Farooq, G. Shen, S. Hu, Kinetic and mechanistic investigations of the degradation of sulfachloropyridazine in heat-activated persulfate oxidation process, Chem. Eng. J. 346 (2018) 515–524, https://doi.org/10.1016/j.cej.2018.04.068.
[61] C. Tan, N. Gao, Y. Deng, Y. Zhang, M. Sui, J. Deng, S. Zhou, Degradation of antipyrine by UV, UV/H_2O_2 and UV/PS, J. Hazard. Mater. 260 (2013) 1008–1016, https://doi.org/10.1016/j.jhazmat.2013.06.060.
[62] X. Lou, L. Wu, Y. Guo, C. Chen, Z. Wang, D. Xiao, C. Fang, J. Liu, J. Zhao, S. Lu, Peroxymonosulfate activation by phosphate anion for organics degradation in water, Chemosphere 117 (2014) 582–585, https://doi.org/10.1016/j.chemosphere.2014.09.046.
[63] Z. Wang, Y. Shao, N. Gao, X. Lu, N. An, Degradation kinetic of phthalate esters and the formation of brominated byproducts in heat-activated persulfate system, Chem. Eng. J. 359 (2019) 1086–1096, https://doi.org/10.1016/j.cej.2018.11.075.
[64] S. Wu, H. Li, X. Li, H. He, C. Yang, Performances and mechanisms of efficient degradation of atrazine using peroxymonosulfate and ferrate as oxidants, Chem. Eng. J. 353 (2018) 533–541, https://doi.org/10.1016/j.cej.2018.06.133.
[65] M. Xu, J. Li, Y. Yan, X. Zhao, J. Yan, Y. Zhang, B. Lai, X. Chen, L. Song, Catalytic degradation of sulfamethoxazole through peroxymonosulfate activated with expanded graphite loaded $CoFe_2O_4$ particles, Chem. Eng. J. 369 (2019) 403–413, https://doi.org/10.1016/j.cej.2019.03.075.
[66] L. Lai, H. Zhou, B. Lai, Heterogeneous degradation of bisphenol A by peroxymonosulfate activated with vanadium-titanium magnetite: performance, transformation pathways and mechanism, Chem. Eng. J. 349 (2018) 633–645, https://doi.org/10.1016/j.cej.2018.05.134.
[67] X. Duan, Z. Ao, L. Zhou, H. Sun, G. Wang, S. Wang, Occurrence of radical and nonradical pathways from carbocatalysts for aqueous and nonaqueous catalytic oxidation, Appl. Catal. B Environ. 188 (2016) 98–105, https://doi.org/10.1016/j.apcatb.2016.01.059.
[68] Y. Feng, J. Liu, D. Wu, Z. Zhou, Y. Deng, T. Zhang, K. Shih, Efficient degradation of sulfamethazine with $CuCo_2O_4$ spinel nanocatalysts for peroxymonosulfate activation, Chem. Eng. J. 280 (2015) 514–524, https://doi.org/10.1016/j.cej.2015.05.121.
[69] S. Al Hakim, S. Jaber, N.Z. Eddine, A. Baalbaki, A. Ghauch, Degradation of theophylline in a UV254/PS system: matrix effect and application to a factory effluent, Chem. Eng. J. 380 (2020), 122478, https://doi.org/10.1016/j.cej.2019.122478.
[70] Y. Feng, Q. Song, W. Lv, G. Liu, Degradation of ketoprofen by sulfate radical-based advanced oxidation processes: kinetics, mechanisms, and effects of natural water matrices, Chemosphere 189 (2017) 643–651, https://doi.org/10.1016/j.chemosphere.2017.09.109.
[71] G.P. Anipsitakis, D.D. Dionysiou, Radical generation by the interaction of transition metals with common oxidants, Environ. Sci. Technol. 38 (2004) 3705–3712, https://doi.org/10.1021/es035121o.
[72] S. Su, W. Guo, Y. Leng, C. Yi, Z. Ma, Heterogeneous activation of Oxone by $CoxFe_{3-x}O_4$ nanocatalysts for degradation of rhodamine B, J. Hazard. Mater. 244 (2013) 736–742, https://doi.org/10.1016/j.jhazmat.2012.11.005.
[73] X. Li, Z. Wang, B. Zhang, A.I. Rykov, M.A. Ahmed, J. Wang, $FexCo_{3-x}O_4$ nanocages derived from nanoscale metal–organic frameworks for removal of bisphenol A by activation of peroxymonosulfate, Appl. Catal. B Environ. 181 (2016) 788–799, https://doi.org/10.1016/j.apcatb.2015.08.050.
[74] L. Pi, N. Yang, W. Han, W. Xiao, D. Wang, Y. Xiong, M. Zhou, H. Hou, X. Mao, Heterogeneous activation of peroxymonocarbonate by Co-Mn oxides for the efficient degradation of chlorophenols in the presence of a naturally occurring level of bicarbonate, Chem. Eng. J. 334 (2018) 1297–1308, https://doi.org/10.1016/j.cej.2017.11.006.
[75] L. Li, C.G. Niu, H. Guo, J. Wang, M. Ruan, L. Zhang, C. Liang, H.Y. Liu, Y.Y. Yang, Efficient degradation of Levofloxacin with magnetically separable $ZnFe_2O_4$/NCDs/Ag_2CO_3 Z-scheme heterojunction photocatalyst: vis-NIR light response ability and mechanism insight, Chem. Eng. J. 383 (2020), 123192, https://doi.org/10.1016/j.cej.2019.123192.

[76] A. Kaur, D.B. Salunke, A. Umar, S.K. Mehta, A. Sinha, S.K. Kansal, Visible light driven photocatalytic degradation of fluoroquinolone levofloxacin drug using Ag_2O/TiO_2 quantum dots: a mechanistic study and degradation pathway, New J. Chem. 41 (2017) 12079–12090, https://doi.org/10.1039/C7NJ02053H.
[77] X. Liu, Y. Liu, S. Lu, Z. Wang, Y. Wang, G. Zhang, X. Guo, W. Guo, T. Zhang, B. Xi, Degradation difference of ofloxacin and levofloxacin by UV/H_2O_2 and UV/PS (persulfate): efficiency, factors and mechanism, Chem. Eng. J. 385 (2020), 123987, https://doi.org/10.1016/j.cej.2019.123987.
[78] K. Xu, W. Ben, W. Ling, Y. Zhang, J. Qu, Z. Qiang, Impact of humic acid on the degradation of levofloxacin by aqueous permanganate: kinetics and mechanism, Water Res. 123 (2017) 67–74, https://doi.org/10.1016/j.watres.2017.06.037.
[79] K.H. Wammer, A.R. Korte, R.A. Lundeen, J.E. Sundberg, K. McNeill, W.A. Arnold, Direct photochemistry of three fluoroquinolone antibacterials: norfloxacin, ofloxacin, and enrofloxacin, Water Res. 47 (2013) 439–448, https://doi.org/10.1016/j.watres.2012.10.025.
[80] Y. Xia, Q. Dai, Electrochemical degradation of antibiotic levofloxacin by PbO_2 electrode: kinetics, energy demands and reaction pathways, Chemosphere 205 (2018) 215–222, https://doi.org/10.1016/j.chemosphere.2018.04.103.
[81] X.J. Wen, C.G. Niu, H. Guo, L. Zhang, C. Liang, G.M. Zeng, Photocatalytic degradation of levofloxacin by ternary Ag_2CO_3/CeO_2/AgBr photocatalyst under visible-light irradiation: degradation pathways, mineralization ability, and an accelerated interfacial charge transfer process study, J. Catal. 358 (2018) 211–223, https://doi.org/10.1016/j.jcat.2017.12.005.
[82] M.R. Abukhadra, A. Helmy, M.F. Sharaf, M.A. El-Meligy, A.T.A. Soliman, Instantaneous oxidation of levofloxacin as toxic pharmaceutical residuals in water using clay nanotubes decorated by ZnO (ZnO/KNTs) as a novel photocatalyst under visible light source, J. Environ. Manag. 271 (2020), 111019, https://doi.org/10.1016/j.jenvman.2020.111019.